Building Tomorrow's Society

Bâtir la Société de Demain

Fredericton, Canada

June 13 – June 16, 2018/ *Juin 13 – Juin 16, 2018*

EFFECTS OF LOW TEMPERATURE AND HIGH STRAIN RATE ON THE COMPRESSIVE BEHAVIOUR OF CONCRETE

MacLean, Thomas J.[1,3] and Lloyd, Alan[2]
[1] University of New Brunswick, Canada
[2] University of New Brunswick, Canada
[3] tom.maclean@unb.ca

Abstract: Explosions and large impacts are dangerous to structures due to their high force and impulsive nature. When combined with the effects of extreme temperature, the structure can be pushed to its limits, which could result in a catastrophic failure. The research presented here is a preliminary investigation into this largely unexplored design scenario, focusing primarily on the effects of low exposure temperature and high strain rates on concrete materials. The primary purpose of the research was to experimentally determine strength increase factors that incorporate the combined effects of low temperature and high strain rates on the compressive behaviour of concrete. A total of eighteen 101.6 mm x 203.2 mm (4" x 8") concrete cylinders were tested in uniaxial compression under static and dynamic strain rates at the University of New Brunswick. Static loads were applied by a compression machine and dynamic loads were applied by a drop mass impactor. The specimens were exposed to four different temperatures from +20°C to -70°C by means of placing them in a regulated freezer or a dry ice environmental chamber to cool. The vertical strain of the specimens during testing was determined by using Digital Image Correlation (DIC). A high-speed camera was used to monitor the dynamic tests. Stress – strain curves were generated for all static and dynamic samples, allowing for direct comparisons of peak stress and strain between the test conditions. Design equations and relationships between the dynamic increase factor (DIF), temperature increase factor (TIF) and combined increase factor (CIF) are presented.

1 INTRODUCTION

Concrete is a material that has been used in structures for centuries, yet there is still uncertainty concerning its material properties in certain situations. Many researchers have performed high exposure temperature research for the purpose of fire resistance. However, there has not been sufficient experimental work to confidently determine the resulting changes in the behaviour of structural properties due to the exposure of low temperatures, especially in tandem with high strain rates. Examples of some of the applications of the research would be dynamically loaded concrete structures exposed to the cold Canadian climate, where temperatures can be found to be less than -50 °C (National Research Council of Canada, 2015) or in storage facilities where liquid natural gas and other industrial materials are contained (Dahmani et al. 2009).

Literature shows that increasing strain rates results in an increase of the compressive strength of concrete (Bischoff and Perry 1991 & 1995, Hughes and Watson 1978, Ross et al. 1996). Additionally, this strength increase is also shown when exposure temperatures are lowered (Lee et al. 1988, Xie et al. 2014). However, there is little information about the combined effects of both high strain rates and low

temperatures, especially at strain rates around 1 s^{-1}. 1 s^{-1} is an accepted typical far field flexural strain rate for flexural concrete design and will be used as a reference magnitude in this study (CSA Group 2012).

This paper describes an experimental research program designed to investigate this scenario. A summary of results of concrete tested under static and dynamic loads while exposed to low temperatures is presented. Design equations and relationships between the dynamic increase factor (DIF), temperature increase factor (TIF) and combined increase factor (CIF) are presented. The factors determine the relative increase in compressive strength observed due to temperature and strain rate influenced tests in comparison to static tests performed at room temperature.

2 EXPERIMENTAL PROGRAM

Eighteen 101.6 mm x 203.6 mm (4"x8") concrete cylinders were tested in uniaxial compression for the experimental program. Twelve concrete cylinders were tested under static conditions while being exposed to various low temperatures at the University of New Brunswick, while the remaining six were loaded dynamically. The testing temperatures used were 20, -10, -40 and -70 °C.

2.1 Specimen Preparation

A concrete mix design was tailored to produce a design target compressive strength (f_c') of 30 MPa. Portland cement and fly ash were combined with water to produce a water/cementitious material ratio of 0.45. Fine aggregate accounted for 43% of the total aggregate for the mix, which had a maximum size of 19.05 mm. The mix design proportions used are shown in Table 1.

Table 1: Mix design proportions

Material	Mix density (kg/m^3)
Portland cement	180
Fly ash	180
Water	162
Coarse aggregate	1035
Fine aggregate	781

Standard 101.6 mm x 203.6 mm concrete cylinder molds were used for mold preparation. However, as being able to monitor the internal temperature of specimens was necessary, modifications to the cylinder molds were required. A 3.4 mm steel wire was cut into 127 mm rods and placed through two small drilled holes located at mid height on opposite sides of the sleeve to stay in position. Two T-type high performance thermocouple wires were then put through one of the holes in the side of the mold and were taped to the rod so that the thermocouple contact points were located at the centre of the cylinder and at half of the radius, as shown in Figure 1. This spacing allowed a thermal gradient to be determined during the testing of each specimen. This was primarily incorporated for static tests, as the room temperature increased the surface temperature of chilled specimens much quicker than the core temperature. To overcome this difference, the measured temperature of both thermocouples throughout the test were averaged to determine the overall test temperature.

2.2 Exposure Temperatures

The desired temperature groups for the experiment were +20, -10, -40 and -70 °C. The 20 °C group was used as control samples, as it represented typical room temperature. Specimens required to reach -10 °C were placed in a freezer until their temperature stabilized. The colder temperatures of -40 and -70 °C were outside the working range of the freezer, therefore a dry ice environmental chamber was created. The chamber submerges cylinders in dry ice as shown in Figure 2. Dry ice sublimates at a temperature of -78.5 °C, therefore it is an ideal material for this test. The exposed ends of the embedded thermocouples protrude the cover of the environmental chamber, therefore temperatures can be monitored and specimens can be removed once desired temperatures are reached.

Figure 1: Concrete sleeve layout

Figure 2: Dry ice environmental chamber

2.3 Static Compression Test Setup

Twelve static uniaxial compression tests were performed on cylinders by a compression machine, shown in Figure 3. The specimens were loaded with a continuous stress rate of 0.25 MPa/s, resulting in an average static strain rate of 20 $x10^{-6}$ s^{-1}. The exposure temperatures used were 20, -10, -40 and -70 °C. Three compression tests were performed at each temperature interval and average responses were obtained. The static compression tests performed at 20 °C were considered as the control specimens for the entire experimental program. A typical static test setup is shown in Figure 4.

Figure 3: Compression machine

Figure 4: Static test setup

Stress-strain relationships were obtained for each test. Vertical strain data was acquired by using 3D DIC. Load values were obtained from the compression machine at the same rate and time as the images taken, allowing for simple data alignment of stress and strain. The thermocouples of the specimens were connected to a multimeter and the temperature from both thermocouples was taken at the beginning of the test and after failure. The freezer and dry ice environmental chamber specimens underwent an increase of roughly 1.5 °C and 4 °C throughout the tests respectively due to interaction with room temperature.

2.3.1 3D Digital Image Correlation

The vertical displacement of the specimens during compression testing was determined by 3D DIC. DIC is a non-contact optical technique that can be used to monitor strain and displacement that is simple to use and more accurate than manual measurement methods (McCormick and Lord 2010). DIC works by comparing numerous digital photographs taken of a specimen throughout the expected deformation period of a test by tracking the movement of specific blocks of pixels over time (McCormick and Lord 2010). The DIC system that was implemented with static testing was a two camera system that allowed for 3D imaging, as seen in Figure 5. The pair of cameras working in unison provides full-field 3D deformation and strain data. The cameras were set to operate at 5 fps.

DIC systems work most effectively when each of the individual pixel blocks being monitored are random with a large range of contrast and intensity levels (McCormick and Lord 2010). The randomness and contrast levels were obtained by painting the surface of the test samples a matte white and then speckling the surface with flat black spray paint. Matte colours are used to reduce the reflections seen and optimize the data collection process. An example of a speckled sample is shown in Figure 6.

Figure 5: 3D DIC camera setup

Figure 6: Static - speckled cylinder

2.4 Dynamic Compression Test Setup

Six dynamic uniaxial compression tests were performed on concrete cylinders that were loaded by a drop mass impactor, shown in Figure 7. A 740 kg steel sled shown in Figure 8 was raised and then allowed to freefall 1.5 m onto a concrete cylinder with a 101.6 mm x 38.1 mm cylindrical piece of wood on top. The wood was inserted to reduce the applied strain rates of the system by reducing the overall system stiffness. It was intended to have the low velocity impacts produce strain rates of 0.5 – 2 s^{-1}. Figure 9 shows a typical test setup of the cylinder and wooden interface material above one of the load cells for the dynamic tests.

Figure 7: Drop mass impactor

Figure 8: Drop mass sled

Figure 9: Dynamic test setup

2.4.1 Load Data

The applied load produced from the impact of the sled and the specimen was measured using two load cells. The load cells were designed to have a capacity of 1450 kN and were calibrated based on the compression machine used for static testing. Data acquisition software was used to monitor both load cells at a rate of 25 kHz. One load cell was placed below the specimen, while the other was attached to the bottom of the drop mass sled. An average of both load cells was taken to determine the average applied load to the specimen over time.

2.4.2 High Speed Camera

The vertical strain of the specimens during the dynamic compression testing was determined by using 2D DIC with a high speed camera. The single camera was set to take images at a rate of 20 kHz. A distinct difference between the speckling patterns of the cylinder for static and dynamic tests can be observed in Figure 6 and Figure 9. Due to the high frame rate of the high speed camera, the image resolution had to be reduced. This resulted in larger speckles needing to be used, as there were fewer pixels to monitor for DIC purposes. The speckle patterns on the dynamic specimens were applied manually by randomly applying dots using a dry permanent marker dipped in matte black paint.

3 EXPERIMENTAL RESULTS

The experimental results focus on the change in material properties of concrete due to the varying factors of temperature and strain rate. The primary objective is to determine the effects that these factors have on the stress – strain response of ordinary concrete.

3.1 Static Results

A typical stress-strain relationship obtained from the axial compression testing of cylinders at static load rates is shown in Figure 11. The curve has four different points labelled on the plot, which correlate to the adjacent images in Figure 10. The different colour gradients show the applied strain on the concrete at that point of the test. Virtual extensometers were placed vertically along the specimen and an average vertical strain was determined for each photograph. The average strain was paired with the analog stress data obtained from the testing machine to create the stress-strain plots for each test.

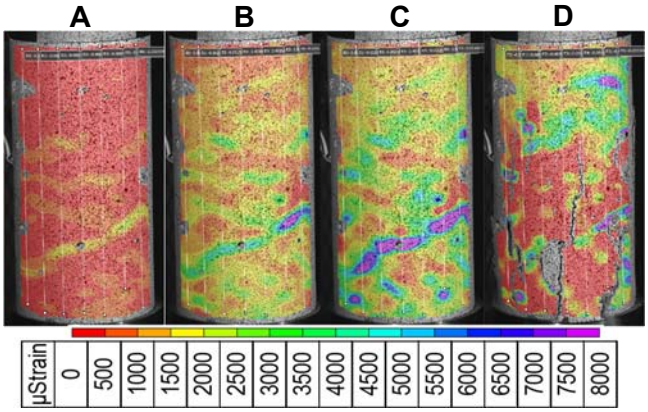

*F*igure 10: Strain data images during testing

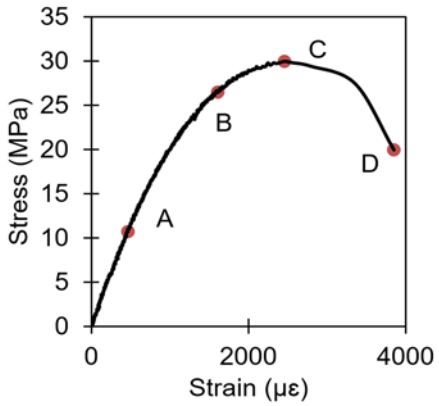

Figure 11: 20C-S3 - Stress vs. strain

The four temperature groups each had three specimens tested statically and the resulting stress-strain curves were plotted together in Figure 12. The concrete material properties of interest are the peak stress and associated peak strain. In addition to the experimental data, Hognestad's curve was included in each plot of Figure 12 as a solid line (Hognestad et al. 1955). Equation 1 was used to develop this theoretical curve, which was calculated using the average peak values for stress and strain of each temperature group.

$$[1]\ \sigma = \begin{cases} f_c' \left[\frac{2\varepsilon}{\varepsilon_0} - \left(\frac{\varepsilon}{\varepsilon_0}\right)^2\right], & \varepsilon < \varepsilon_0 \\ f_c' \left[1 - 0.15\left(\frac{\varepsilon - \varepsilon_0}{\varepsilon_u - \varepsilon_0}\right)\right], & \varepsilon_u \geq \varepsilon \geq \varepsilon_0 \end{cases}$$

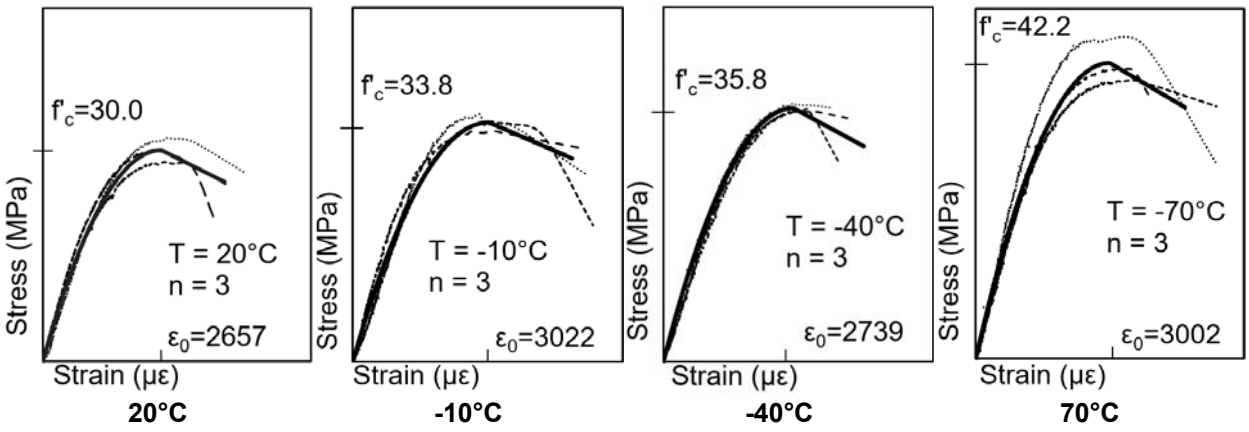

Figure 12: Static compression stress vs. strain plots

The four plots in Figure 12 are based off the same horizontal and vertical scales, which show the significant increase in compressive strength observed as temperature decreased. The largest strength gain occurred when temperatures were decreased to -70 °C, resulting in an average strength gain of 41% compared to the control samples. The calculation of the temperature increase factor and static peak strain ratio are shown in Equation 2 and Equation 3 respectively. It should be noted that there was not a linear increase in brittleness due to the lower exposure temperatures as previous literature suggested (Xie et al. 2014). A summary of the average group properties from the static tests is shown in Table 2.

[2] TIF = $\frac{f'_{cT}}{f'_{c20}}$

[3] Temperature Peak Strain Ratio = $\frac{\varepsilon_{0,T,s}}{\varepsilon_{0,20,s}}$

In Equation 2, f'_{cT} is the average compressive strength of the desired temperature group and f'_{c20} is the average compressive strength of the 20 °C group. In Equation 3, $\varepsilon_{0,T,s}$ is the average peak strain of the desired temperature group and $\varepsilon_{0,20,s}$ is the average static peak strain of the 20°C group.

Table 2: Static axial compression test results summary

Average Group Property	20 °C	-10 °C	-40 °C	-70 °C
f'_c (MPa)	29.97	33.83	35.79	42.24
ε_o (με)	2657	3022	2872	3002
AVG temperature (°C)	22.6	-10.1	-41.2	-68.1
TIF	1	1.13	1.20	1.41
Temperature peak strain ratio	1	1.14	1.03	1.13

A linear increase was observed in the temperature increase factor for each group as temperature decreased. The peak values for stress and the associated average testing temperature for each test is shown in Figure 13. The linear relationship shows the increase in strength due to decreasing the exposure temperature of concrete at static rates.

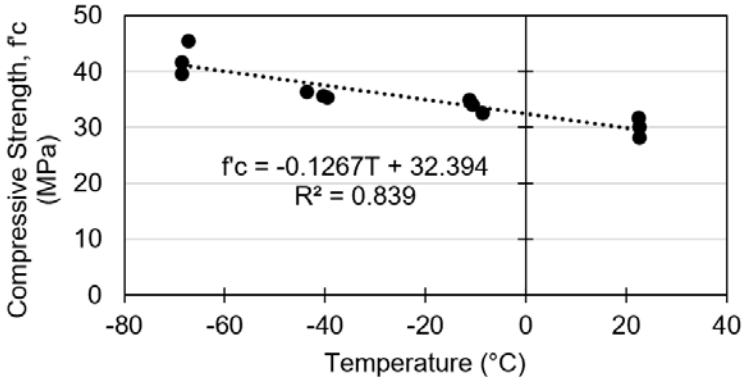

Figure 13: Static compressive stress vs. temperature

3.2 Dynamic Results

Figure 17 shows the typical member response to dynamic loads by the Drop Mass Impactor. Stress was measured over time by the two load cells and the average value was taken. Strain was measured using DIC over time by placing a minimum of three virtual extensometers on the concrete surface and taking the average for each photograph. A sample of images taken by the high-speed camera and the strain data extraction of a typical test is shown in Figure 14. The average strain values from each of the four images are shown in Figure 15. The two measurement systems produced Figure 15 and Figure 16 independently. The two systems were aligned by determining the frame of impact and the first load increase. This time alignment allowed for the generation of the stress-strain curve of a cylinder loaded dynamically.

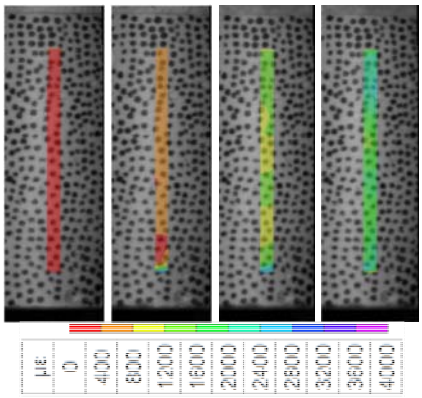

Figure 14: 20C D1 – Sample strain images

Strain vs. Time

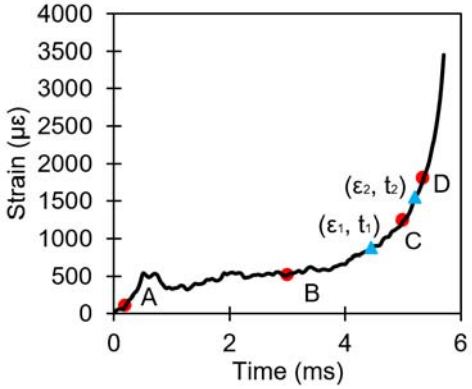

Figure 15: 20C D1 - Strain vs. time

Stress vs. Time

Stress vs. Strain

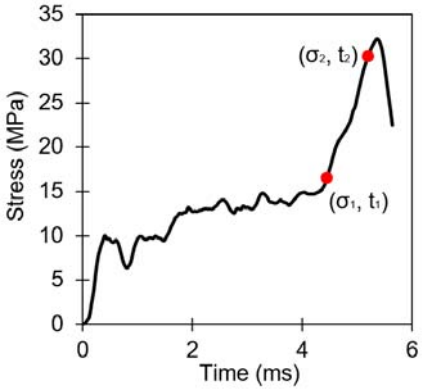

Figure 16: 20C D1 - Stress vs. time

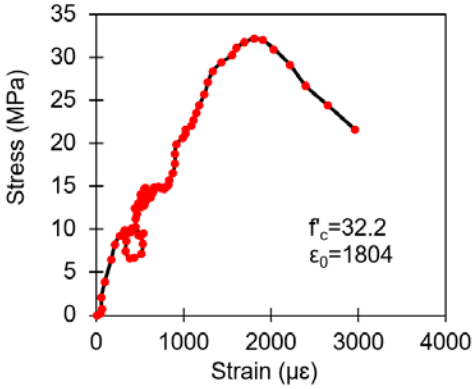

Figure 17: 20C D1 - Stress vs. strain

The horizontal plateaus in Figure 15 and Figure 16 from roughly 1-4 ms are due to the impact with the wooden interface material. This interface material caused noise in the stress-strain data due to the high density of points. However, the material was required to reduce the overall stiffness of the setup to maintain strain rates in the magnitude of 0.5-2 s^{-1}. The average strain rate for dynamic testing was 1.21 s^{-1}. One additional trial was conducted using a steel interface instead; this resulted in the strain rates being above 10 s^{-1} due to steel's high stiffness. The effects of the wooden material can be observed until roughly 15 MPa in the previous plots. After this point, the wooden material had reached its deformation limit and only the concrete deformed. The DIC strain measurements only consider concrete deformation during the test.

Strain rates were determined by taking two points on the stress vs. time plots after the plateau from the wood crushing when the response was essentially linear due to concrete being the sole contributor to deformation. The associated strain values were taken and divided by the time between the points. This is a linear approximation, as the strain rate was not constant. The calculation used to determine strain rate is shown in Equation 4. Sample points for calculating strain rates are shown in Figure 15 and Figure 16.

[4] $\dot{\varepsilon} = \frac{\varepsilon_2 - \varepsilon_1}{t_2 - t_1}$

Temperature, dynamic and combined increase factors can be determined through examining the peak stress values of the dynamic and static tests at various temperatures. Equation 5 and Equation 6 show the calculations of the dynamic and combined increase factors.

[5] DIF = $\frac{f'_{cTd}}{f'_{cTs}}$

[6] CIF = $\frac{f'_{cTd}}{f'_{c20s}}$

In Equation 5, f'_{cTd} is the average compressive strength of a desired temperature group loaded dynamically and f'_{cTs} is the average compressive strength of the same temperature group loaded statically. In Equation 6, f'_{cTd} is the peak compressive strength of a desired temperature group loaded dynamically and f'_{c20s} is the peak compressive strength of the 20 °C group loaded statically.

Figure 18 shows the temperature increase factors for static loads and the combined increase factors for dynamic loads. The highest average combined increase factor was 1.61, which occurred to the dynamically loaded specimens exposed to -70 °C. Dynamic loads for the 20 °C samples had an average dynamic increase factor of 1.15.

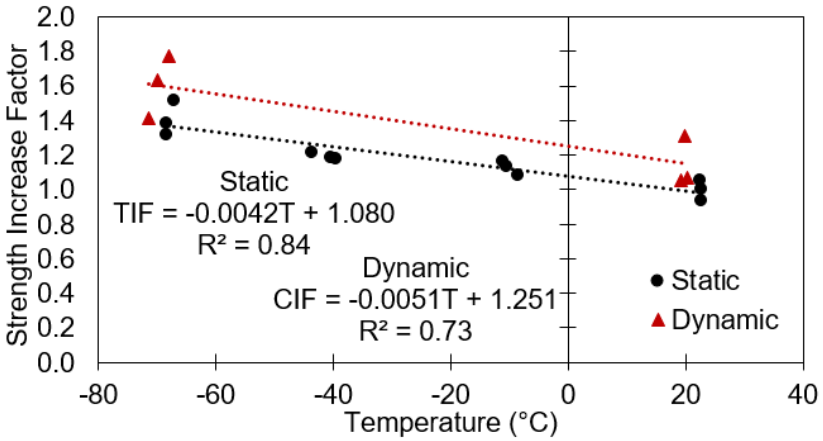

Figure 18: Increase factor vs. temperature

Even though there was not any significant change in peak strain for static tests exposed to different temperature, there was an apparent increase in brittleness due to the application of dynamic loads. Equation 7 shows the calculation for the dynamic peak strain ratio. Relative to the static tests of the same temperature, the dynamic tests for 20 and -70 °C had dynamic peak strain ratios of 0.71 and 0.72 respectively. There were variations in the dynamic strain rates of tests by $\pm$ 0.45 s^{-1}. This small difference was deemed acceptable to allow for direct comparisons between the tests. Table 3 shows a summary of all dynamic test properties monitored and the associated factors.

[7] Dynamic Peak Strain Ratio = = $\frac{\varepsilon_{0,T,d}}{\varepsilon_{0,T,s}}$

In Equation 7, $\varepsilon_{0,T,d}$ is the average peak strain of a temperature group loaded dynamically and $\varepsilon_{0,T,s}$ is the average peak strain for the same temperature group loaded statically.

Table 3: Dynamic axial compression test results summary

Average Group Property	20 °C	-70 °C
f'_c (MPa)	34.38	45.71
ε_0 (με)	1896	2171
DIF	1.15	1.14
Temperature (°C)	19.8	-69.8
TIF	1	1.40
CIF	1.15	1.61
Dynamic peak strain ratio	0.71	0.72
Strain rate (s^{-1})	1.34	1.08

4 ANALYSIS

Analysis was performed by comparing the experimentally determined strength increase factors amongst themselves to determine apparent relationships. The experimental test results correlated to produce design equations that are presented. In addition, the test results are compared to past literature.

4.1 Strength Increase Factors

Important results from the experimental program are the magnitudes of the temperature, dynamic and combined strength factors. Table 4 shows a summary of all of the strength increase factors obtained in the experimental program for 20 and -70 °C.

Table 4: Strength Increase Factors

Load Type	Property	20 °C	-70 °C
Static	TIF_S	1	1.41
Dynamic	DIF	1.15	1.14
	TIF_D	1	1.40
	$(DIF)(TIF_D)$	1.15	1.60
	CIF	1.15	1.61

Table 4 shows that the magnitude of the DIF was not dependent on exposure temperature, as the samples had essentially the same increase factor of 1.15 and 1.14 for the 20 °C and -70 °C groups respectively. Additionally, the TIF was not dependent on the applied strain rate, as the samples had essentially the same increase factor of 1.41 and 1.40 for static and dynamic loads respectively. Lastly, an interesting relationship can be determined for the CIF, as the value obtained experimentally can be effectively obtained by multiplying the DIF and TIF, as shown in Equation 8. This was applicable for both data sets quite accurately, as shown in Table 4. This would allow for design scenarios involving the combined effects of strain rate and low temperature to be tested independently and then combine the strength increase factors based on Equation 8. This finding would greatly simplify future test procedures.

[8] CIF = (DIF)(TIF)

4.2 Design Equations

Equation 9 and Equation 10 are the two design equations presented for determining the increase in compressive strength of a specimen due to low temperatures, impact strain rates and the combined effects.

[9] TIF = -0.0042T + 1.080

[10] CIF = -0.0051T + 1.251

These design equations are applicable for exposure temperatures of 20 °C to -70 °C, strain rates of the magnitude of 1 s^{-1} and a static compressive strength of roughly 30 MPa.

4.3 Comparisons to Literature

The experimental program results reinforce the notions that compressive strength increases when exposed to temperature and strain rates are increased independently (Bischoff and Perry 1991 & 1995, Hughes and Watson 1978, Ross et al. 1996, Lee et al. 1988, Xie et al. 2014). It should be noted that there has been large variations in magnitudes of increases for both scenarios in literature.

Shourky et al. (2011) presented a linear equation for static compressive strength based on exposure temperatures from -30°C to +60 °C, which had a slope of -0.13. The experimental trend line for static compressive stress as a function of temperature in Figure 13 showed a very similar slope of -0.127. It is reasonable to assume that slope of the equation found by Shourky et al (2011) would continue if tested at lower temperatures, thus agreeing with the experimental values found for static temperature effects.

Filiatrault and Holleran (2001) and Qiao et al. (2016) have both performed dynamic compression tests exposed to low temperatures. Filiatrault and Holleran (2001) saw an average CIF of 1.91 when a rate of 0.1 s^{-1} was applied to a specimen while exposed to a temperature of -40 °C. Meanwhile, Qiao et al. (2016) saw an average CIF of 1.5-1.63 when strain rates of 33-63 s^{-1} were applied while exposed to temperatures of -75 °C. The obtained CIF results from the experimental program land between values of both studies.

5 CONCLUSIONS

Based on the preliminary test results obtained, the following conclusions can be made about the combined effects of low exposure temperature and hard impact strain rates.

- The dynamic increase factor does not appear to be effected by temperature changes. The strength increase between the dynamic and static tests of the same temperature was the same regardless of temperature, with factors of 1.15 and 1.14 respectively due to average strain rates of 1.2 s^{-1}.
- The temperature increase factor does not appear to be influenced by varying strain rates. The strength increase observed between the 20 °C and -70 °C samples remained the same regardless if it was loaded statically or dynamically, with increase factors of 1.40 and 1.41 respectively.
- The combined effects of low exposure temperature and increasing strain rates was essentially equal to multiplying the observed DIF and TIF. The largest increase resulted in a CIF = 1.61.
- The dynamic peak strain ratio comparing the dynamic peak strain of a cylinder to the static peak strain of the same temperature was the same regardless of temperature. The 20 °C and -70 °C samples had peak strain ratios of 0.71 and 0.72 respectively, resulting in more brittle failures.

Further testing is required to determine the combined effects of low exposure temperature and high strain rates. The effects of applying higher strain rates (10 – 100 s^{-1}) to the test specimens at low temperatures, the effects of the moisture content of specimens during combined effects tests and the influence of static compressive strength on the magnitude of strength increases observed should be investigated in the future.

References

Bischoff, P.H. and Perry, S.H. 1991. Compressive Behaviour of Concrete at High Strain Rates. *Materials and Structures,* **24**(6): 425-450.

Bischoff, P.H. and Perry, S.H. 1995. Impact Behaviour of Plain Concrete Loaded in Uniaxial Compression. *Journal of Engineering Mechanics,* **121**(6): 685-693.

CSA Group. 2012. Design and Assessment of Buildings Subjected to Blast Loads. Mississauga, Ontario, Canada.

Dahmani, L., Khennane, A. and Kaci, S. 2007. Behavior of the Reinforced Concrete at Cryogenic Temperatures. *Cryogenics,* **47**(9): 517-525.

Filiatrault, A. and Holleran, M. 2001. Stress-Strain Behaviour of Reinforcing Steel and Concrete Under Seismic Strain Rates and Low Temperatures. *Materials and Structures,* **34**(4): 235-239.

Hughes, B.P. and Watson, A.J. 1978. Compressive Strength and Ultimate Strain of Concrete under Impact Loading. *Magazine of Concrete Research,* **30**(105): 189-199.

Hognestad, E., Hanson, N.W., and McHenry, D. 1955. Concrete Stress Distribution in Ultimate Strength Design. Journal of the American Concrete Institute, 52(12), 455-480.

Lee, G.C., Shih, T.S. and Chang, K.C. 1988. Mechanical Properties of Concrete at Low Temperature. *Journal of Cold Regions Engineering,* **2**(1): 13-24.

National Research Council of Canada. (2015) *National Building Code of Canada 2015*, National Research Council of Canada, Ottawa, Ontario, Canada.

McCormick, N. and Lord, J. 2010. Digital Image Correlation. *Materials Today,* **13**(12): 52-54.

Qiao, Y., Wang, H., Cai, L., Zhang, W. and Yang, B. 2016. Influence of Low Temperature on Dynamic Behaviour of Concrete. *Construction and Building Materials,* **115**: 214-220.

Ross, A.C., Jerome, D.M., Tedesco, J.W. and Hughes, M.L. 1996. Moisture and Strain Rate Effects on Concrete Strength. *Materials Journal,* **93**(3): 293-300.

Shourky, S.N., William, G.W., Downie, B. and Raid, M.Y. 2011. Effect of Moisture and Temperature on the Mechanical Properties of Concrete. *Construction and Building Materials,* **25**(2): 688-696.

Xie, J., Li, X. and Wu, H. 2014. Experimental Study on the Axial-Compression Performance of Concrete at Cyrogenic Temperatures. *Construction and Building Materials,* **72**: 380-388.